Integrated design of flight simulator motion cueing systems

R. Hosman
Aerospace Man-Machine Systems Consulting BV
Delfgauw, The Netherlands

S. Advani
Simulation & Training, Aircraft Development & Systems Engineering BV
Hoofddorp, The Netherlands

N. Haeck
Mathematics and Motion Control Specialist, Hellevoetsluis, The Netherlands

ABSTRACT

An advanced design process applicable to the specification of flight simulator cueing systems is presented in this paper. This process is based on the analysis of the pilot-vehicle control loop by using a pilot model incorporating both visual and vestibular feedback, and the aircraft dynamics. After substituting the model for the simulated aircraft, the analysis tools are used to adjust the washout filter parameters with the goal of restoring pilot control behaviour. This process allows the specification of the motion cueing algorithm. Then, based on flight files representative of the operational flight envelope, the required motion system space is determined. The motion-base geometry is established based on practical limitations, as well as criteria for the stability of the platform with respect to singular conditions. With this process the characteristics of the aircraft, the tasks to be simulated, and the missions themselves are taken into account in defining the simulator motion cueing system.

NOMENCLATURE

e	attitude error
$f_{x,y,z}$	specific force along X, Y and Z axis
g	gravity
H	transfer function
i	forcing function signal
J	cost function
n	normal load
Q, R	weighting factors
r	sensory output
u	pilot's control output
w	disturbance signal
W	weighting factor
y	controlled system output
δ	control output
φ	roll angle
φ_m	phase margin
θ	pitch angle
τ_i	information processing time delay
ω	frequency
ω_c	crossover frequency
ω_n	natural frequency of the neuromotor system
ζ	damping coefficient

Subscripts

p	pilot
c	controlled system
I	information processing
Man	manoeuvre task
Dist	disturbance task
C, rate	central visual system, rate perception
C, att	central visual system, attitude perception
SCC	semicircular canals
s	simulator
vis	visual
vest	vestibular

Paper No. 2756. Manuscript received 11 December 2002, revised version received 18 January 2004, accepted 19 November 2004.

https://doi.org/10.1017/S000192400000049X Published online by Cambridge University Press

1.0 INTRODUCTION

Since the introduction of the synergistic six-degrees-of-freedom motion platform, many flight simulators have been designed, built and deployed for training and research applications. The choice of the system characteristics is based on the requirements of the simulator user and, if applicable, regulatory requirements. The major part of the motion system requirements, in particular the motion space, system bandwidth, maximum load, etc. are actually dependent upon the operation required to be simulated. The current lack of motion cueing criteria, however, is the primary reason that there has been no real progress in the development of motion cueing algorithms and the systematic design of simulator motion systems during the last decades. As a result, the final specifications are primarily based on experience, rather than the training need.

Teunissen[1] in his paper during the conference on 'Can flight simulation do everything?' argued that for the selection of the training means from CBT (Computer based training) to FFS (Full flight simulator), it is necessary to first specify the training objective (the level of proficiency that the trainee has to master), and the training need (the difference between the objective, and the proficiency before the training). If the selection of the FFS is based on such a specification, then the motion system characteristics must still be specified. It is known that the flight manoeuvres to be simulated, and the properties of the motion cueing algorithm, determine the required motion space of the motion system.

In an effort to change this status quo, Advani and Hosman[2] presented a scheme for an integrated design of the motion cueing algorithm and the motion system, Fig. 1. Based on this strategy, the specification of both the motion cueing algorithm (also known as the washout filter) and the motion system geometry can be specified if the required knowledge, information and software are available.

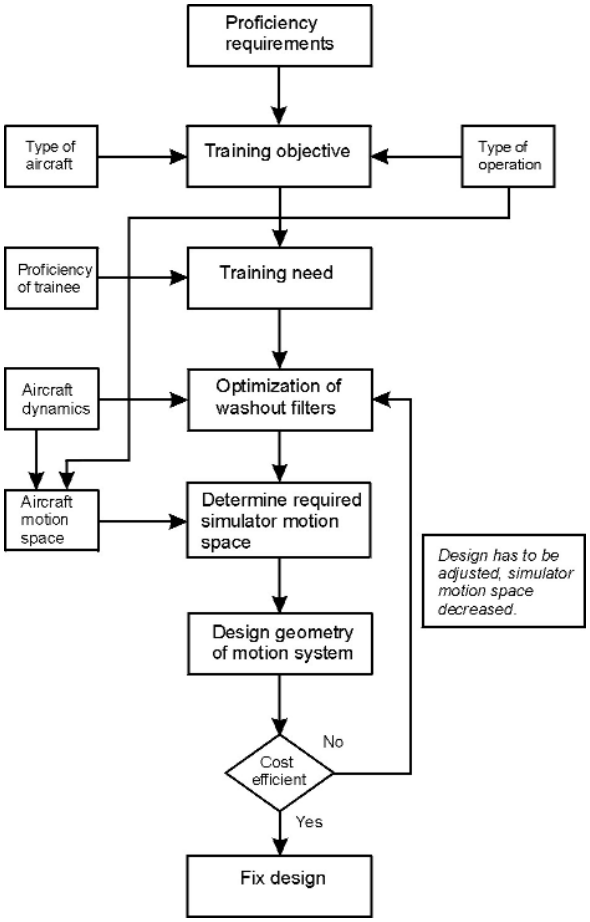


Figure 1. Motion-cueing system design process (Advani-Hosman, 2000[2]).

Since the presentation of the paper in 2000, several customers have shown interest in the integrated design method. Several projects to design these washout filters, the motion system geometry and the combined integrated design of the motion system and washout algorithm have been performed since (Ref. 3), or are currently in progress.

The present paper will discuss the details, merits and shortcomings of the design procedure, based on an example employing a generic fighter aircraft. First an overview of the process and its building blocks will be presented. Thereafter, the results of the example are shown and discussed. Finally, after a discussion of the results, conclusions are drawn.

2.0 SIMULATOR MOTION CUEING SYSTEM DESIGN PROCESS AND ELEMENTS

The authors have developed systematic means of specifying simulator motion cueing systems, comprised the motion drive algorithm and the motion-base mechanism. The design process follows four essential steps:

1. Adjust a validated pilot model to the given dynamics of the aircraft.
2. Introduce simulator parameters (time delays and washout filter form), and adjust the washout algorithm parameters in order to restore the pilot-simulator system behaviour as closely as possible to the pilot-aircraft behaviour.
3. Based on the stabilised pilot-simulated aircraft system, generate ideal simulator trajectories representing characteristic manoeuvres.
4. Design a simulator motion-base that contains these trajectories.

The integrated design is based on a sequential analysis, which leads to the optimisation of the motion cueing algorithm and the geometry of the motion system. For the analysis, the following models are required:

1. An aerodynamic model of the aircraft.
2. A model describing a pilot's skill-based control behaviour incorporating the visual and vestibular feedback.
3. A model describing a pilot's motion perception incorporating visual and vestibular stimulation.
4. A model describing the general form of the motion cueing algorithm.
5. A set of (simulated) flight files covering the operation to be simulated.
6. Software to transform aircraft motion to simulator motion.
7. A tool to optimise the design of the motion system, including a means of comparing the actual available workspace with that required by the above simulations.

In the generic fighter example discussed in this paper, linear models will be used. This is not a requisite, but for the analysis based on non-linear models, more detailed information and knowledge is required, and the analysis itself is much more extensive. Both the aircraft model and the flight files derived from a simulation trial were used with permission of the National Aerospace Laboratory NLR in Amsterdam.

As described by Hosman[4], a distinction must be made regarding the influence of motion feedback at each of the three different levels of behaviour as described by Rasmussen[5]. These levels are skill-based (manual control), rule-based and knowledge-based behaviour.

https://doi.org/10.1017/S000192400000049X Published online by Cambridge University Press

2.1 Pilot-model adaptation to the aircraft-model

The first step in the analysis is to adapt the pilot model to the aircraft dynamics in the attitude control loop, Fig. 2. The pilot model used in this type of analysis must be able to process the influence of the visual and vestibular feedback (Hess,[6], Hosman,[7,8]) in the inner attitude control loop on the pilot's skill-based manual control behaviour. Based on extensive research on the influence of visual and vestibular perception of motion stimuli, and on motion perception and control behaviour in tracking tasks, a descriptive pilot model has been developed and validated (Hosman,[7,8]. The aim was to attain a model capable of describing the influence of the visual and vestibular stimulation induced by the aircraft motions on a pilot's control behaviour. The final model is depicted in Fig. 3.

With the experiments described by Hosman, the dynamics of the sensors and the interaction between the visual and the vestibular systems were evaluated. In this model, the human motion sensors, each described by a transfer function, are placed in parallel and convert the stimuli – the attitude, angular rate, and angular acceleration – to the sensory outputs $R_i(\omega)$. The differences in sensor dynamics are due to the fundamental differences between the visual and the vestibular system: The visual system is position and rate sensitive, while the vestibular system is sensitive to angular accelerations and specific forces.

In the perception and decision process, the many sensory outputs have to be integrated into a single output. Based on the experimental results during tracking tasks, the model output is generated by a weighted sum of the sensory outputs. Each individual weighting factor W_i emphasises the contribution of each sensory output.

Next, the time delays resulting from the information processing and the neuromuscular system are incorporated into the model.

Owing to the high bandwidth character of a well-designed neuromotor-manipulator control system ($\omega_n >> \omega_c$), the information processing delay and the neuromotor-manipulator system can be modelled by one single lumped time delay τ_I. Taking into consideration the effective time delay of the human operator in tracking tasks (McRuer and Jex,[9], and the characteristics of the visual system, Hosman (1996) set $\tau_I = 0{\cdot}2$s. This value is valid for tracking tasks with a side stick as the manipulator, and system dynamics that allow a high closed-loop bandwidth ($\omega_c >>$ 3rad/sec). For system dynamics corresponding with those of transport aircraft, a larger time delay and neuromuscular dynamics (that account for the influence of the aircraft control system) have to be incorporated within the model. This is a result of the adaptation of pilot's control behaviour to the slower dynamics of transport aircraft.

When a pilot adjusts his/her behaviour to a certain control task, the first objective is to achieve an acceptable level of tracking performance. The tracking performance can be quantitatively assessed using the mean square value of the tracking error. When the pilot tries to minimise the tracking error alone, his control actions do not take into account the aircraft characteristics, structural loads and passenger comfort, for example. Therefore, if the mean square error were the only component of the cost function used to adapt the model to the aircraft dynamics, this would drive the model parameters to a value for best performance regardless of the effect on the dynamic characteristics of the closed loop. In reality, the pilot will normally consider putting more effort into the task as a function of the benefit of the resulting performance improvement, and relative to the corresponding increase in workload. For these reasons, to bring the workload effect

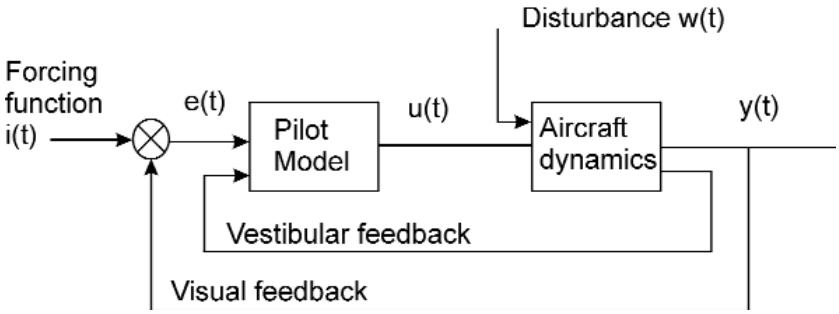


Figure 2. The closed loop with the pilot and the aircraft and the visual and vestibular feedback loops.

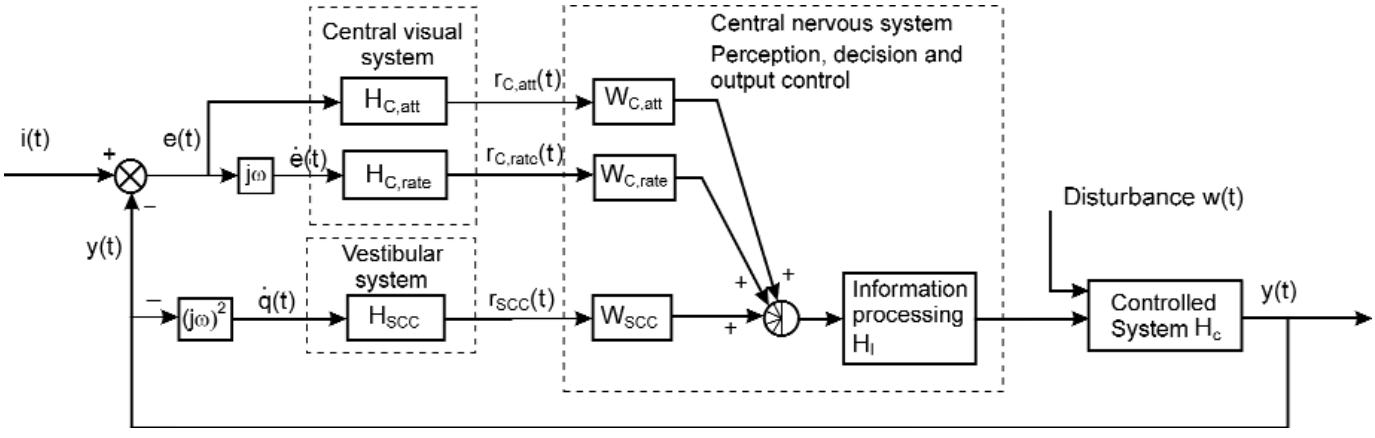


Figure 3. Block diagram of the descriptive pilot model in the manoeuvre task.

https://doi.org/10.1017/S000192400000049X Published online by Cambridge University Press

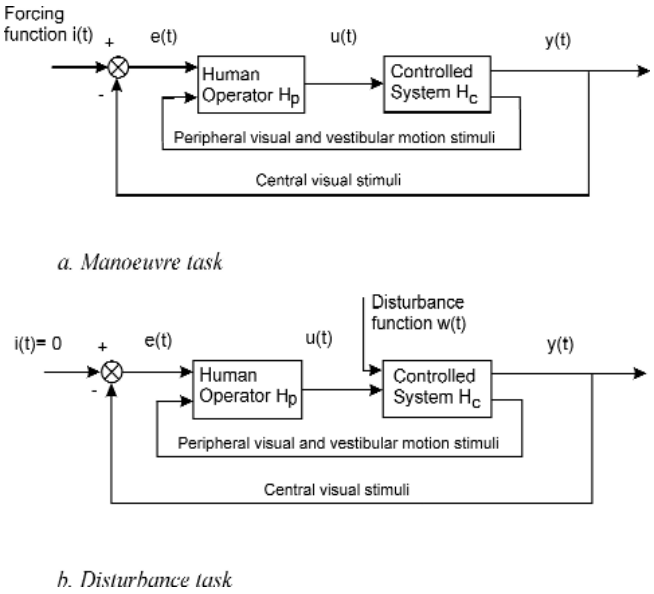


Figure 4. Differences in the influence of motion feedback in the manoeuvre task and the disturbance task.

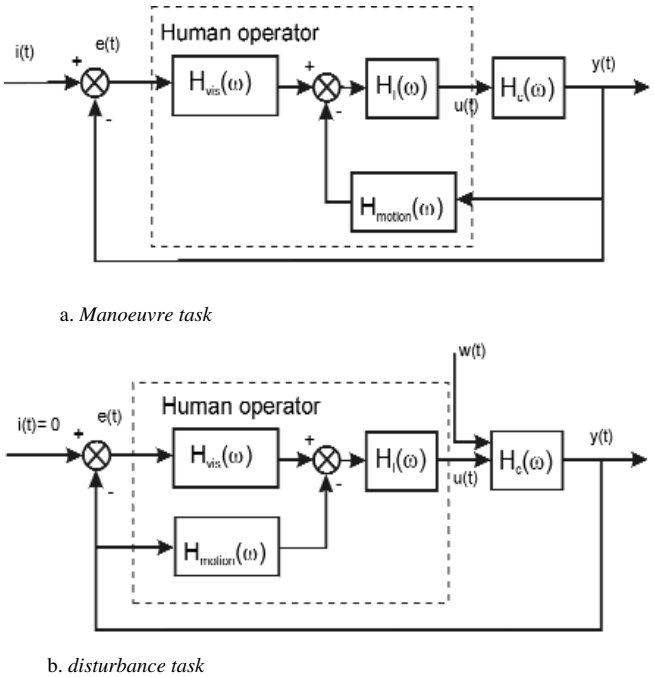


Figure 5. Simplified scheme of the pilot model in the closed loop for the manoeuvre and the disturbance task.

into account, the mean square of the control signal and its derivative have to be added to the cost function.

There is another consideration: When a pilot tries to improve tracking performance, he will also increase his gain. This will result in an increase of the crossover frequency ω_c and a decrease in phase margin φ_m. A gain that is too high will reduce the stability of the control loop. So, the choice of the cost function should aim at the following:

- Good tracking performance
- Effective control effort
- Adequate bandwidth and stability of the control loop as expressed by the crossover frequency and the phase margin

In order to achieve these goals, the following cost function can be applied.

$$J = \Sigma(e^2 + Q.\,\delta^2 + R.\,\dot{\delta}^2) \quad \ldots(1)$$

Where e is the attitude tracking error, and δ is the control output. By incorporating the control output δ and its derivative $\dot{\delta}$ the control effort and its bandwidth are taken into account. The weighing factors Q and R in the cost function depend primarily on the aircraft characteristics, and on the task to be performed, i.e. the disturbance or manoeuvre task.

2.2 Task dependence

With this model, the influence of visual and vestibular motion feedback upon the manoeuvre task and the disturbance task can be described. The advantage of using the model is that by describing the influence of the visual and vestibular feedback on a pilot's control behaviour, the only free model parameters are the sensory weighting coefficients W_i, Fig. 3.

In Fig. 4 two control-loops are shown. In the first, the manoeuvre task, pilot's control is directed to minimise the tracking or attitude error $e(t)$ when making the aircraft follow the external reference or forcing function. In the second, the disturbance task, pilot's control is aimed to minimise the attitude error $e(t)$ due to the external disturbance as turbulence. These two tasks have a different influence on pilot's control behaviour. This difference is increased by motion feedback. The transfer-function describing pilot's control behaviour is defined as:

$$H_p(\omega) = \frac{U(\omega)}{E(\omega)} \quad \ldots(2)$$

Depending on the task, manoeuvre task versus disturbance task, the transfer function can be derived as follows. In Fig. 5 the pilot model of Fig. 3 with the visual and vestibular feedback is simplified to three transfer functions $H_{vis}(\omega)$, $H_{motion}(\omega)$, and $H_I(\omega)$. In this figure $y(t)$ is the aircraft attitude. In the manoeuvre task the attitude error $e_1(t) = i(t) - y(t)$, while in the disturbance task $e_2(t) = -y(t)$.

In the case of the manoeuvre task the motion feedback forms an additional feedback loop which leads to:

$$H_{p,Man}(\omega) = \frac{H_{vis}(\omega)H_I(\omega)}{1 + H_{motion}(\omega)H_I(\omega)H_c(\omega)} \quad \ldots(3)$$

For the disturbance task $H_{vis}(\omega)$, and $H_{motion}(\omega)$ contribute to the control output in parallel. Hence the control behaviour is described by:

$$H_{p,Dist}(\omega) = (H_{vis}(\omega) + H_{motion}(\omega)).H_i(\omega) \quad \ldots(4)$$

When these transfer functions are worked out for the full pilot model of Fig. 3, then the following transfer functions for pilot's control behaviour in the manoeuvre and disturbance task can be derived:

$$H_{p,Man}(\omega) = \frac{[W_{C,att}.H_{C,att}(\omega) + W_{C\,rate}.H_{C\,rate}(\omega).j\omega]}{[1 + W_{SCC}.H_{SCC}(\omega).(j\omega)^2.H_I(\omega).H_c(\omega)]}.H_I(\omega). \quad \ldots(5)$$

https://doi.org/10.1017/S000192400000049X Published online by Cambridge University Press

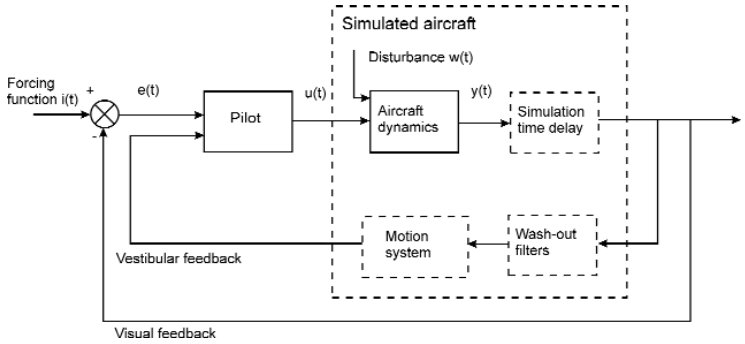


Figure 6. The pilot simulated-aircraft control loop.

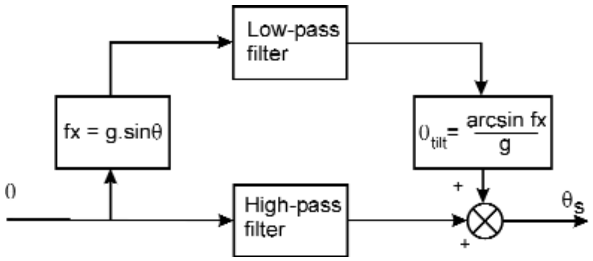


Figure 7. Simplified scheme of the washout influence on the simulation of the pitch angle. The specific force f_x equals gsinθ in steady, straight, symmetric flight.

and

$$H_{p,Dist}(\omega) = [W_{C,att}.H_{C,att}(\omega) + W_{C\,rate}.H_{C\,rate}(\omega).j\omega + W_{SCC}.H_{SCC}(\omega).(j\omega)^2].i$$

$$H_I(\omega). \quad \ldots (6)$$

The cost function of Equation (1) will be used to adjust the descriptive pilot model to the dynamics of the aircraft. To prevent the adjustment to a minimum of the cost function outside the normal operation area of the pilot, additional constraints may be required in order to attain a practical and sound result of the optimisation.

2.3 Motion washout parameter adjustment

After the pilot model has been adapted to the particular aircraft dynamics, the closed loop of Fig. 1 is adapted to the closed loop of the simulated aircraft, Fig. 6. In this scheme, three elements are added to the pilot-aircraft control loop: a lumped simulation time delay, the washout filter, and the motion system. In the present analysis, it is assumed that the motion system behaves perfectly in terms of its dynamics and so has a gain of unity.

As a result of the changes of the control loop caused by the simulation, the pilot will adapt his behaviour to the simulated-aircraft control loop. Using the pilot and aircraft model as the basis, the washout algorithm parameters are adjusted by hypothesising that the cost function used to adapt the pilot model to the aircraft dynamics indeed describes the pilot's control strategy.

In the end, the motion washout algorithm coefficients remain the only parameters that may be adjusted in this phase. When the transfer function of these algorithms is introduced into the pilot-vehicle system, their coefficients can be adjusted through a mathematical optimisation. In the end, the optimisation should try to restore the pilot control behaviour as closely as possible to the original behaviour. This is accomplished by using the same weighing factors in the cost function *J*, Equation (1), in finding the optimal washout parameters. The resulting control strategy by the pilot can then be maintained in the simulator as it originally was in the aircraft

For the adaptation of the washout filters to the pilot model and aircraft dynamics in the present project, the following arguments have been applied:

For a pilot's skill-based control behaviour, the inner attitude control loops are of direct importance (Hosman,[4]. Therefore, the simulation of the pitch angle and the roll angle are of primary interest. When applying the classical washout filter, the high-pass rotational filter and the low-pass tilt-co-ordination filters generate the pitch and roll angles. The high-frequency components pass through the high-pass filter. The low-frequency components pass through the gravity component g Sin or g Sin of the specific force, and are filtered by the tilt-co-ordination filter. Therefore, the washout filter's influence on the simulated aircraft attitude can be simplified as shown in Fig. 7.

The remaining washout filter parameters, namely the high pass translational filters, have a direct influence on a pilot's rule-based and knowledge based behaviour. For these levels of behaviour, the perception of the aircraft motions in the environment directly impacts the performance. A general motion perception model is required in order to analyse and optimise the translational filters. Such a motion perception model is under development at TNO-Human Factors Institute in Soesterberg, The Netherlands. Bos *et al.* (Ref. 10) applied this model to the motion perception during the take-off run of a transport aircraft. Although further development and evaluation is required, this model may be applied to the optimisation of the translational filters in the washout algorithm. Therefore, in the present analysis the translational filter parameters have to be chosen based on the authors' experience.

In the end, this step generates the required parameters for the motion drive algorithm in order that the pilot perceives and responds to the simulated vehicle in a way that is as similar as possible to the real vehicle. Once the washout algorithm has been established, the required motion space can be determined.

3.0 EXAMPLE: INTEGRATED DESIGN OF A GENERIC FIGHTER SIMULATOR MOTION SYSTEM

3.1 The aircraft model

For this analysis, a linear approximation of a generic fly-by-wire fighter aircraft model has been used. Besides the fact that the full non-linear model could not be made available for this application, the whole analysis with a linear model is less complicated, can be performed in a much shorter time, and has a wider application.

The linear approximation was fitted to the total aircraft model (flight control system and aircraft) for the pitch and roll response to the control input. Based on the response to six sinusoidal input signals with an amplitude one third of the maximum control input, the modulus and phase were determined.

The basic form of the linear model is:

$$H\frac{attitude}{control}(\omega) = \frac{K_c}{j\omega\{(j\omega)^2 + 2\varsigma\omega_0 j\omega + \omega_0^2\}} \quad \ldots (7)$$

and is an approximation of the non-linear aircraft model and the flight control system.

https://doi.org/10.1017/S000192400000049X Published online by Cambridge University Press

Table 1
The linearised aircraft model parameters

Mode	Velocity [kt]	K_c	ω_0 [rad/s]	ζ
Pitch	150	7·9	3·5	1·4
	200	6·5	3·5	0·9
	300	15·5	6·0	1·4
Roll	150	25	4·6	0·7
	200	54·6	5·7	1·06
	300	115	7·2	1·1

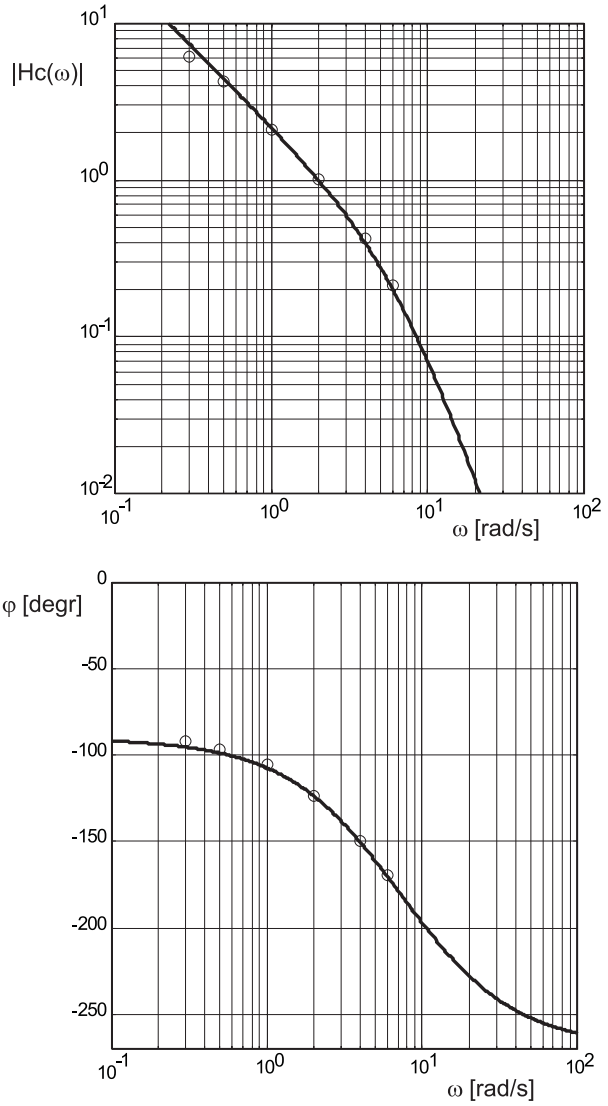


Figure 8. Bode plot of the linearized aircraft model and the frequency response of the non-linear model.

Table 2
Pilot model adjustment, tracking performance and loop closure

Disturbance task	$W_{C,att}$	$W_{C,rate}$	W_{SCC}	Standard deviation error	ω_c	ω_m
Velocity [kt]				[deg]	[rad/s]	[deg]
Pitch						
150	4·830	0	2·723	0·395	2·141	55·68
200	4·453	0	2·135	0·422	2·118	58·62
300	5·225	0	2·252	0·354	1·860	67·32
Roll						
150	3·145	0	0·982	0·621	3·427	42·36
200	3·320	0	0·969	0·598	3·804	39·63
300	3·065	0	0·736	0·654	4·345	36·34

Manoeuvre task	$W_{C,att}$	$W_{C,rate}$	W_{SCC}	Standard deviation error	ω_c	φ_m
Pitch				[deg]	[rad/s]	[deg]
150	0·711	1·578	0	1·199	0·898	98·97
200	1·072	1·345	0	1·212	0·821	97·69
300	1·631	1·507	0	1·158	0·894	91·69
Roll						
150	0·680	0·544	0	1·145	1·155	92·76
200	0·510	0·534	0	1·082	1·670	85·29
300	2·370	0·236	0·813	1·007	1·986	63·84

The linear model was fitted for three velocities: V = 150kt, 200kt, and 300kt. In Fig. 8, an example of the Bode plot of the linear model together with the measured frequency response of the non-linear model are presented.

It is clear from Equation (7) and Fig. 8, the linear model behaves as an integrator at low frequencies. At higher frequencies, the flight control system is no longer capable of maintaining the integrator characteristics, as described by the linear model by the second order term in the denominator of Equation (7).

3.2 Pilot model adaptation

For the pilot model adaptation, the sensory weighting coefficients W_i, Fig. 2, now have to be chosen. This is accomplished by an optimisation procedure using the cost function of Equation (1). When in this procedure a sensory output r_i does not contribute in minimising the costfunction I , the corresponding weighting coefficient W_i will become zero. The Bode plot of the adapted pilot model with and without motion feedback in the disturbance task is presented in Fig. 9. Table 2 presents the model adjustment and closed loop performance. Note that in the pilot model, a small time delay and a second-order system to describe the neuro-motor system dynamics replace the information processing time delay.

From Table 2, it is clear that in the disturbance task (Fig. 5) the pilot model uses only the vestibular feedback, while in the manoeuvre task the visual rate feedback is used. The influence of vestibular feedback in the manoeuvre task depends on the aircraft dynamics, see Equation (5). For this particular aircraft, vestibular feedback is of influence in the roll manoeuvre task at 300kt. Given this result, the washout filter parameters are optimised for the disturbance task.

Washout algorithm parameter optimisation

After the pilot model has been adapted to the aircraft dynamics, the pilot model parameters are fixed, and the pilot simulated-aircraft loop

https://doi.org/10.1017/S000192400000049X Published online by Cambridge University Press

is established, Fig. 6. Now, the parameters of the tilt-co-ordination filter and the high-pass rotation filter can be adapted using the cost function J of Equation (1). In Fig. 10, the cost function is shown with respect to the tilt-co-ordination and rotation filter bandwidth $\omega_n(Lp)$ and $\omega_n(Hp)$, respectively. In most cases the cost function J describes a valley as a function of the break frequencies of the high-pass rotational filter, and the low-pass tilt filter.

After the washout parameters are established, the pilot model is adapted to the simulated aircraft and, subsequently, the pilot model adaptation to the real and the simulated aircraft can be compared. Fig. 11 presents the pilot model in the frequency domain for the real aircraft (*i*) without and (*ii*) with motion feedback, (*iii*) the optimised washout filters as described in this paper, and (*iv*) the filters currently used in a motion-based fighter simulator (at the NSF, see below). The primary simulation delays influencing pilot's control behaviour in the simulator are the host computer delay, the outside visual system delay and the motion system delay. The washout parameters determined are valid for the simulated generic fighter aircraft with a lumped simulation time delay of 70ms.

The National Aerospace Laboratory operates its National Simulation Facility, NSF, a flight simulator for research related to fighter aircraft. The pilot model adapted to the generic fighter model simulated with the NSF washout filter differs considerably with the other model adaptations. This is primarily due to the gains of the NSF washout filter, which for this particular simulation were chosen between 0·2 and 0·3. After applying the washout to the vestibular feedback, Fig. 11, the net effect of the pilot model and the washout is almost equal for the optimal filter and the NSF filter.

Note that lowering the washout gains changes the pilot behaviour because the fact that the pilot has to compensate for the attenuation of the motion feedback.

4.0 REALISING THE MOTION-BASE REQUIREMENTS

Until now, this paper has shown how the pilot model and simulated aircraft model can be integrated in order to specify the required characteristics of the motion drive algorithm. The next step is to define the actual motion space requirements.

During flight, the aircraft moves along a trajectory in six degrees-of-freedom. The pilot-based washout algorithm stimulates the same control behaviour by the pilot as in the aircraft, and transforms this trajectory into smaller overall proportions in order to make ground-based simulation as effective as possible. Since it is some form of the specific forces and angular accelerations that must be reproduced by the simulator motion system (and not the position or velocity of the aircraft, which are synthesised by the flight instruments and outside-world display system), one can create realistic simulation for at least a limited portion of the flight envelope in a ground-based environment.

In order to define objectively the six-degrees-of-freedom motion space that is required, a technique has been developed (Advani,[11,12] by which measured state variables of an aircraft are passed through the motion drive algorithm in order to generate the 'ideal' simulator trajectories. If the drive algorithm has been adjusted to the task and aircraft as reported earlier in this paper, and the manoeuvres are measured under similar flight conditions with the same (or similar aircraft), then a simulator that reproduces these trajectories should generate a perception and control output by the pilot just like in the aircraft. This is the basis of the remainder of this strategy.

In this example, recordings of the simulated generic fighter are passed through the motion drive algorithm for the segments of the flight that may be simulated with relatively low sustained-g accelerations ($0{\cdot}5g < n < 2{\cdot}7g$). The manoeuvres in this example include a normal take-off, a number of low-g flight events, and a landing. The motion drive algorithm input variables (the specific forces and angular accelerations) have then been passed through the filters. The resulting trajectory, representing a six-dimensional time history of

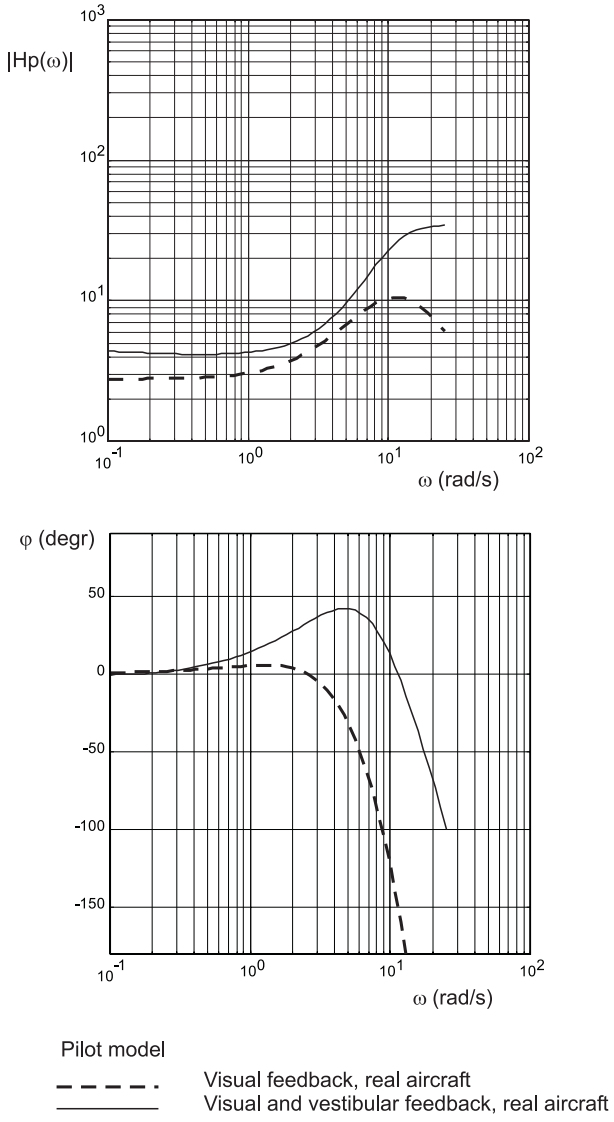


Figure 9. Bode plot of the pilot model for the control of the generic aircraft model in a roll disturbance task at $V = 200$kt.

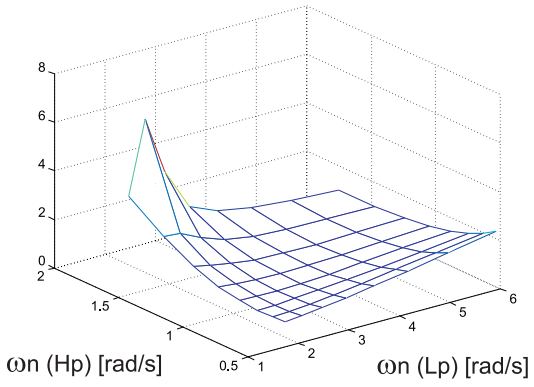


Figure 10. Cost function as a function of the bandwidth of the tilt-co-ordination filter $\omega_n(Lp)$ and of the pitch rotation filter $\omega_n(Hp)$.

https://doi.org/10.1017/S000192400000049X Published online by Cambridge University Press

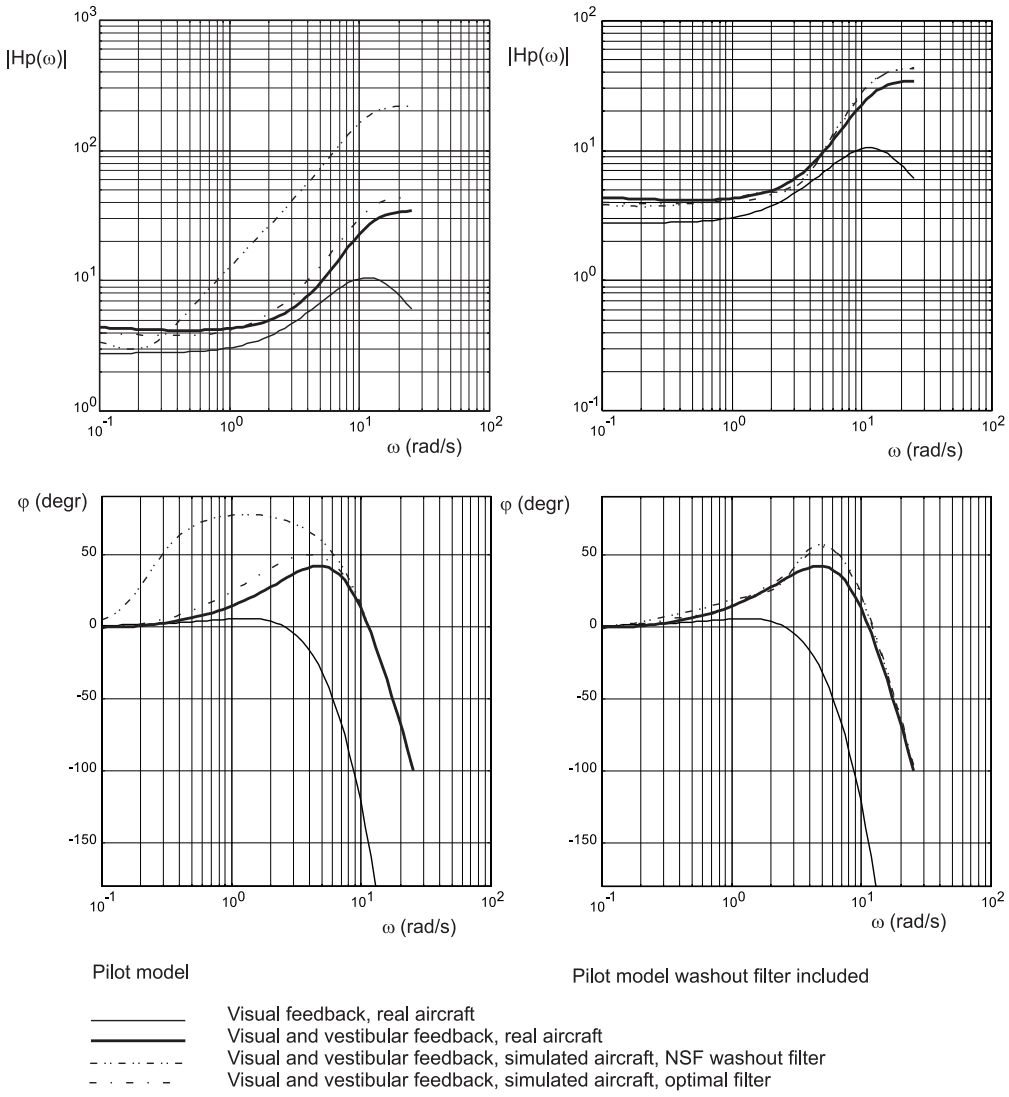


Figure 11. Bode plot of the pilot model for the real aircraft without and with motion feedback and for the simulated aircraft with and without the influence of the washout filter incorporated.

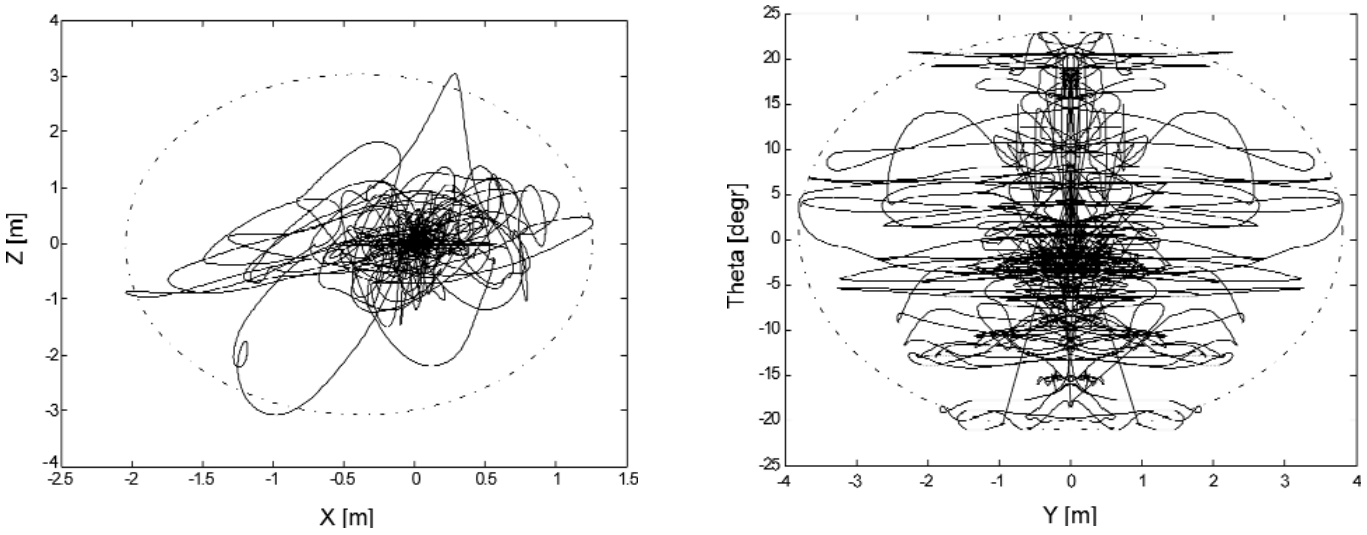


Figure 12. Examples of the trajectories of the simulator motion system due to the flight files of the generic fighter and transformed by the optimal washout filter.

https://doi.org/10.1017/S000192400000049X Published online by Cambridge University Press

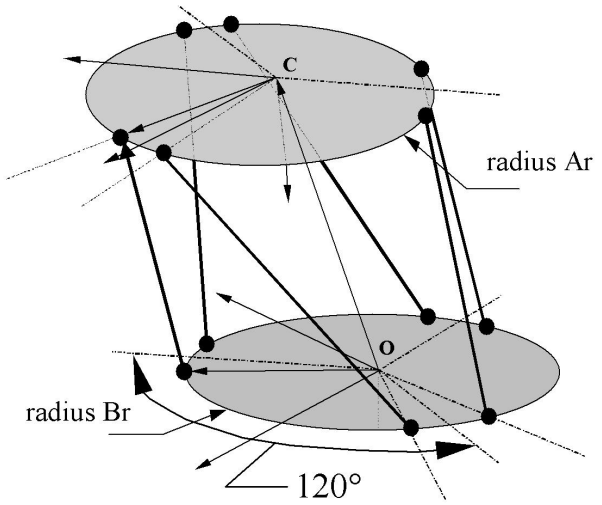


Figure 13. Kinematic representation of the typical circular layout of a conventional Stewart Platform (hexapod) mechanism.

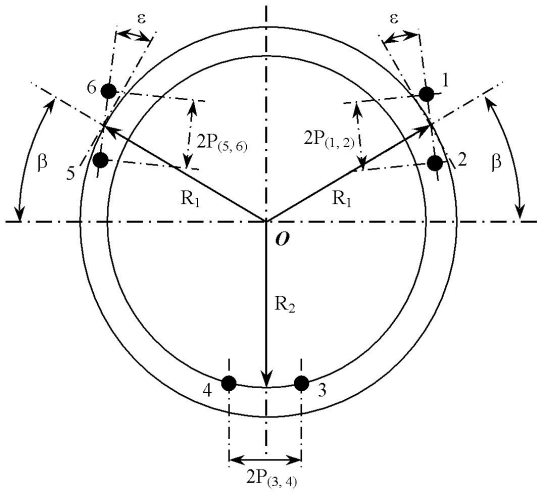


Figure 14. Layout of double-concentric lower platform, where angles β and ε, and dimensions P, R_1 and l_2 are determined by the optimisation. Upper platform has similar optimisation parameters.

simulator motion-base positions and orientations, is then created. Since there are six independent degrees-of-freedom, it is possible to visualize fifteen combinations of the time histories (Surge-Heave, Surge-Sway, Heave-Sway, Pitch-Roll, Pitch-Sway, Pitch-Yaw, Pitch-Surge, etc.)

4.1 Approximation of the trajectories

The trajectories are then encapsulated into a reasonable mathematical approximation, represented by a six-dimensional 'hyper-ellipsoid'. If this ellipsoid contains these trajectories, and if it is possible to manufacture a motion system that is capable of generating a motion envelope at least as large as that ellipsoid, then it is possible to achieve our simulation needs.

Figure 12 shows the trajectories generated by the simulation of the generic fighter aircraft after they were passed through the optimised motion drive algorithm. In total, there are fifteen combinations of the six DOF possible, though we have shown only two for clarity. Note that symmetry is applied to all lateral motions in order to allow the resulting simulator specification to reflect the symmetric capabilities of the aircraft (motions to the left or to the right should be equally possible).

The hyper-ellipsoid generated for these motions is represented in Fig. 12. The size of this ellipsoid is mathematically determined so that the lengths of the primary axes represent the projections of the trajectories along the direction of that axis. In other words, it gives the relative weightings for each of the six degrees-of-freedom. If the trajectories include a large amount of cross coupling, then they will exceed the boundaries of the hyper-ellipsoid. This issue will be resolved in the next section on mechanism design.

Figure 12 also shows that the ellipsoid is not necessarily centred about the zero point in the X and Z degrees-of-freedom. The manoeuvres and resulting trajectories dictate this offset, and one may need to pre-position the simulator prior to a mission or manoeuvre in order to allow its simulation without hitting the actuator travel limits, and without having to over-specify the size of the motion-base.

Table 3 provides the maximum motions in each degree-of-freedom, which were generated by the optimal washout algorithm and trajectory approximation by the hyper-ellipsoid. Note that the trajectories also provide knowledge of the minimum required velocity and accelerations of the motion-base. The design of a tailored motion-base mechanism to suit the requirements is described next.

4.2 Mechanism design

Modern flight simulator motion-bases generally utilise a mechanism known as the Stewart Platform (Stewart,[13] or 'hexapod', which was originally proposed in 1938 for the testing of vehicle tires. This mechanism is comprised of a base-frame, six actuator legs (the jacks), and an upper moving platform, which carries the payload. The legs are attached in pairs, via gimbal joints, to the upper and lower platforms near the vertices of their respective triangular frames.

The hexapod is a mechanically simple, compact and cost-effective system for the generation of motions in up to six simultaneous degrees-of-freedom. It is also easy to install and to maintain. Typically, the locations of the six upper and six lower gimbal joints can be mapped onto circles, and the gimbal pairs are separated by a fixed distance, Fig. 13. The motion of the legs, all six of which are typically identical, is constrained by their minimum and maximum lengths. These constraints impose on the mechanism a kinematic envelope that the upper platform can achieve with respect to the inertial (ground-fixed) reference frame. The six-dimensional envelope of these excursions is the workspace, and determines to a great extent the cueing capability of the simulator. Larger workspace in a given direction (or degree-of-freedom) generally allows longer cue durations. Increasing proportionally the size of all of the members of the Stewart Platform simultaneously extends the maximum translational capabilities of the upper platform, yet will not affect the rotational limits.

The linear actuators of the mechanism can be either hydraulic rams or electric spindle devices. Hexapods are, however, highly limited in workspace when compared to gantry-type systems, for example, the NASA Ames Vertical Motion Simulator. The workspace of a hexapod is also highly coupled. For example, a pitch-up attitude of 20° (common during the simulation of a

Table 3
Hyper-ellipsoid weighting factors generated by the analysis for the generic fighter example for the six degrees of freedom (*X*, *Y*, *Z*, Psi, Theta, and Phi) on the motion platform

X	*Y*	*Z*
± 1·653m	± 3·414m	± 1·786m
Psi	**Theta**	**Phi**
± 8deg	± 22deg	± 17deg

https://doi.org/10.1017/S000192400000049X Published online by Cambridge University Press

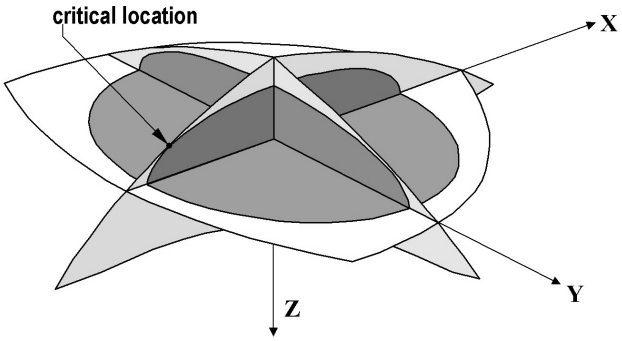


Figure 15. Cross-sectional planes of the translational workspace into which the inscribed ellipse is fit. Optimisation attempts to modify workspace to minimise critical protrusions of ellipses.

take-off) will reduce the available motions in all other directions and rotations to nearly zero.

The performance capability of a motion-cueing system can be characterised by its kinematic envelope (or 'workspace'), and its dynamic characteristics, such as phase delay and damping. These characteristics are a function of the mechanical power available to move the moving platform, its mass properties, and its bandwidth. The motion workspace is, however, a direct function of the architecture of the motion-cueing mechanism.

Using technologies commonly applied in robotic mechanism design, it is feasible to change the layout of the hexapod (thereby deviating from the standard circular arrangement) in order to achieve a greater and better-distributed workspace. For example, one can theoretically place the hinge-points (gimbals) anywhere in space (such as on two concentric, non-coplanar circles, rather than on one; Fig. 14). It is also easy for some manufacturers to change the 'cut-length' of the actuator cylinders and piston rods, while maintaining the original design of the hinge forks, manifolds, cushioning buffers and end blocks. The actuator stroke length may also be specified by the design requirements (rather than arbitrarily chosen multiples of prime numbers, as is often the case).

However, the designer must also prevent the platform from ever achieving a pose (attitude and position) that is at, or close to singularities. In this situation, the ratio of actuator displacements to the resulting platform displacements is very low, meaning that the positioning accuracy may suffer, the mechanical loads can become high, or the control of the system is difficult to achieve.

By using an optimisation programme, all of the above 'free design variables' and constraints can be combined to yield the most suitable architecture tailored to the specified motion envelope.

A method of optimising the motion-base (Advani,[11,12], based on the following steps, was developed and tested. Reference 11, a PhD thesis, should be consulted for more details. The salient points are explained here:

1. Use the basic concept of the Stewart Platform.
2. Establish which geometric parameters should be allowed to vary and by how much, and which should remain fixed.
3. Fit the shape and size of these required motions (as developed earlier in this paper) into the available simulator motions by altering its geometry. This is accomplished through a mathematical optimisation.
4. Check that the leg forces are within reasonable limits, that the legs do not exceed their minimum or maximum lengths, and that the legs do not make physical contact with each other.
5. Iterate if necessary.

Table 4
Optimisation inputs, reduced-gain example

X	*Y*	*Z*
± 0·675m	± 1·378m	± 1·075m
Psi	**Theta**	**Phi**
± 5deg	± 13deg	± 10deg

When combined, the motion trajectories represented a complex pattern of lines, looking perhaps like a ball of steel wool. See Figure 12.

To simplify the process of mathematical optimisation, these patterns were approximated with the six-dimensional hyper-ellipsoid (explained earlier) circumscribing the extremities of the trajectories. In step 3 above, these ellipses are actually inserted into the actual workspace of the mechanism, and this workspace is allowed to 'grow' to the largest possible ellipse to be just contained within its space, Fig. 15. Increasing the workspace and changing its relative shape is made possible by re-locating the hinge points, and changing the characteristics of the actuators, namely their cut lengths.

The final iteration step must not be forgotten. When observing the weighting factors given in Table 3, it is clear that the translational requirements are extremely large, making the application of a hexapod possibly less attractive. By reducing the gains of the translational filters, it is possible to reduce the size of the hyper-ellipsoid to relax the motion-base requirements. Moreover, one can also use the pilot model-based analysis to verify the quality of the resulting simulator.

Since the initial analysis required a very large motion envelope, the washout gains were attenuated by a factor of 0·60 as a demonstration. This generated an ellipsoid with major axis having the dimensions given in Table 4.

Then, the parameters of the hexapod, as described in Figure 16, were optimised in order to contain the resultant hyper-ellipsoid of Table 4. The workspace of the system was indeed re-shaped to accommodate the requirement. The actuator stroke length became 2·115 m (83·27 inches), and the workspace increased in volume by 95 percent over an off-the-shelf system with a 72-inch stroke. Most importantly – although minor, the changes to the geometry ensure that the shape is tailored to the simulation need, based on the pilot model, the vehicle dynamics, and the manoeuvres that are flown.

The workspace and general layout of the final system is shown in Fig. 16. Note that the vertical location of the lower joints is not co-planar, which allows more optimisation freedom. It does mean though, that the forward joints are located lower on the platform than the aft sets. When settled or in the neutral pose (actuators at mid-stroke), the upper hinge points are oriented in a virtual plane having a pitch angle of 22°. While this may seem unusual, it is simply the result of the allowed free design variables, and may be adjusted during subsequent iterations.

Note that these results show ONE possible solution; the actual design effort would yield several options, and the designer must then choose the most viable outcome.

5.0 DISCUSSION AND CONCLUSIONS

The aforementioned process has demonstrated how one can specify the motion cueing algorithm and geometry of a flight simulator motion-base in an objective way.

While the latest scientific knowledge in motion perception and in motion-base design technologies have been applied here, the development of this analytical process is still in progress.

The general motion perception model discussed herein must be developed further before it can be applied to this type of analysis. Subsequently, with this perception model, the full use of the analysis will make it possible to determine the parameters of the high-pass linear motion filters as well.

https://doi.org/10.1017/S000192400000049X Published online by Cambridge University Press

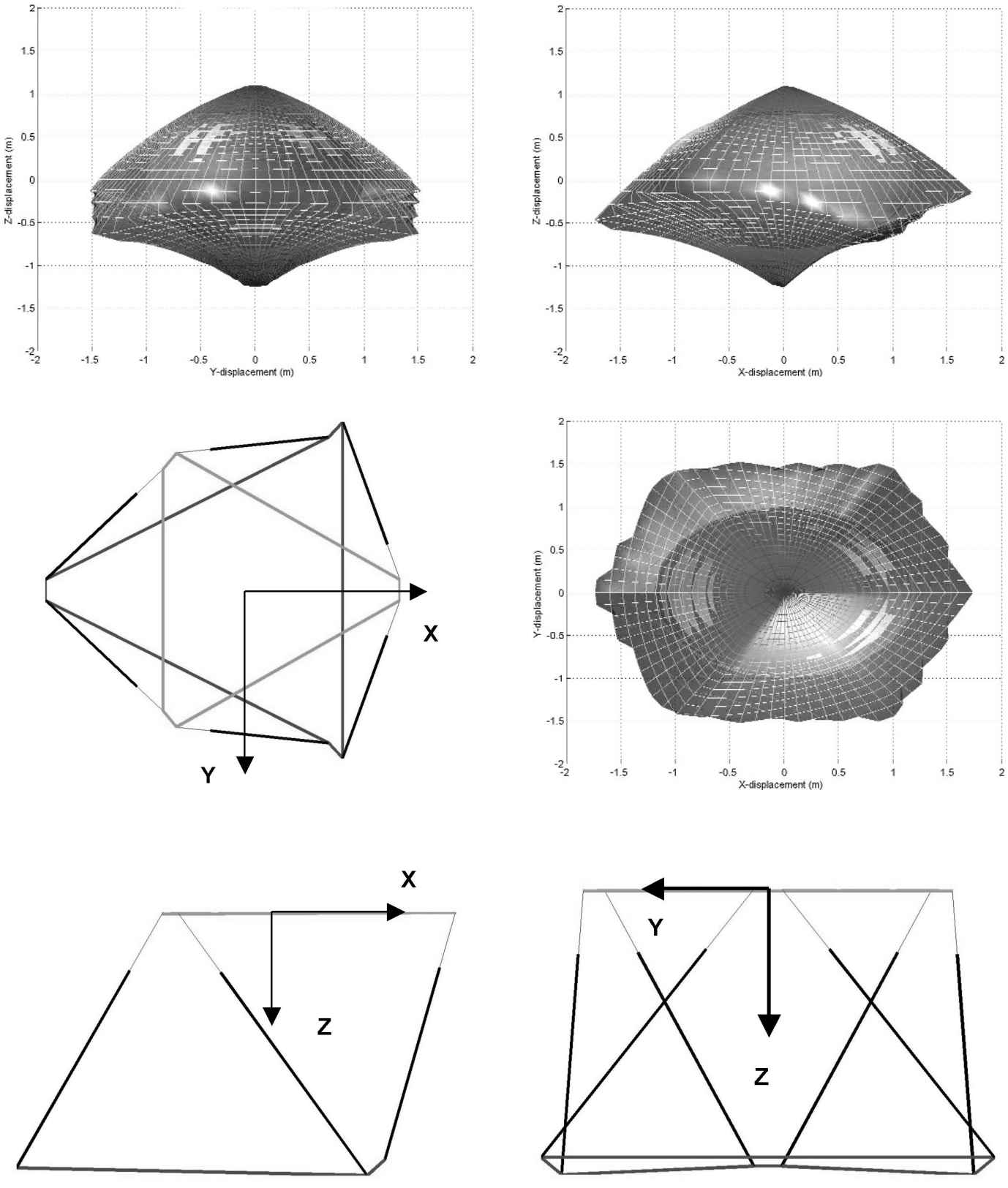


Figure 16. Workspace (translational shown) and geometry of optimised motion-cueing mechanism for the generic fighter simulator example.

https://doi.org/10.1017/S000192400000049X Published online by Cambridge University Press

Support for further research is required in order to evaluate and fully validate the optimal washout filters as demonstrated in this paper. In addition, support is necessary to continue the development of motion perception models.

The washout filter parameters obtained so far are indeed promising. By making a correct choice of the washout parameters, the pilot's control behaviour can be restored very closely to that in real flight.

By using a representative set of flight files, the required motion system space representative for the intended simulator operation can be obtained before the motion system is designed. A feedback of the results of the design into the analysis can be used to fine-tune the final washout algorithm and motion system. In an actual design exercise, this feedback must consider the procurement and exploitation cost of the system, and the general consequences for the design of the simulation facility.

The fact remains that this process allows the designer to achieve the most suitable washout characteristics and motion system performance, within the capabilities of the mechanical hardware. Cost-benefit studies can then be carried out to yield the 'best' solution for the end-user.

In conclusion:

- The integrated motion cueing algorithm and motion-based design discussed in this paper are possible and ready for application.
- A fully validated motion perception model will extend the results of the analysis and further improve the design methodology.
- By applying the presented design methodology, a motion cueing system and algorithm can be tailored to the intended simulation operation.

ACKNOWLEDGEMENTS

The authors thank ADSE BV as well as the NLR, in particular Ir. Alex Rutten, for supporting this study.

6.0 REFERENCES

1. TEUNISSEN, R. The Future of simulation and training. Proceedings of the Royal Aeronautical Society Flight Simulation Conference, Can flight simulation do everything. London, 19-20 May 1999.
2. ADVANI, S.K. and HOSMAN, R.J.A.W. Integrated motion cueing algorithm and motion-base design for flight simulation. proceeding of the conference on: Flight simulation – The next decade. Royal Aeronautical Society, London, 10-12 May, 2000.
3. ADVANI, S.K., GIOVANNETTI, D. and BLUM, M. Design of a hexapod motion cueing system for the NASA Ames Vertical motion simulator. To be presented at the AIAA Modeling & Simulation Technologies Conference, Monterey, CA, USA August 2002.
4. HOSMAN, R. Are criteria for motion cues and time delays possible? AIAA Modeling and Simulation Technologies Conference. Portland, Oregon, USA, 9-11 August, 1999. AIAA CP-99-4028.
5. RASMUSSEN, J. Skills, rules, and knowledge; signals, signs, and symbols, and other distinctions in human performance models. *IEEE Transactions on Systems, Man and Cybernetics*, May/June 1983, **SMC-13**, (3).
6. HESS, R.A. A Model for the human's use of motion cues in vehicular Control. *J of Guidance, Control and Dynamics*, 1990, **13**, (2), pp 476-482.
7. HOSMAN, R.J.A.W. Pilots Perception and Control of Aircraft Motion. PhD Thesis, Delft University of Technology, November 1996. ISBN 90-407-1384-7.
8. HOSMAN, R. and STASSEN, H. Pilot's perception in the control of aircraft motions. *Control Engineering Practices*, 1999, **7**, (11), pp 1421-1428.
9. MCRUER, D.T. and H.R. JEX, A review of quasi-linear pilot models. *IEEE Transactions on Human Factors in Electronics*, September 1967, **HFE-8**, (3).
10. BOS, J.E., BLES, W. and HOSMAN, R.J.A.W. Modeling human Spatial orientation and Motion Perception. AIAA Modeling and Simulation Technologies Conference. Montreal, 6-9 August, 2001. AIAA 2001-4248.
11. ADVANI, S.K. The Kinematic Design of Flight Simulator Motion-Bases. PhD Thesis, Delft University of Technology. Delft University Press, 1998. ISBN 90-407-1672-2.
12. ADVANI, S.K., NAHON, M. and HAECK, N. Optimisation of six-degrees-of-freedom flight simulator motion systems. *AIAA J. Aircr*, September-October 1999, **36**, (5).
13. STEWART, D. A Platform with six-degrees-of-freedom, *Proc Inst of Mechanical Engineers*, 1965-1966, **180**, part 1, (5), pp. 371-386.

https://doi.org/10.1017/S000192400000049X Published online by Cambridge University Press